Stiffness Analysis and Design of a Compact Modified Delta Parallel Mechanism

Robotica (2004) volume 22, pp. 463–475. © 2004 Cambridge University Press
DOI: 10.1017/S0263574704000050 Printed in the United Kingdom

Stiffness Analysis and Design of a Compact Modified Delta Parallel Mechanism

Woo-Keun Yoon*, Takashi Suehiro*, Yuichi Tsumaki† and Masaru Uchiyama‡

(Received in Final Form: November 18, 2003)

SUMMARY
In our previous work, we developed a compact 6-DOF haptic interface as a master device which achieved an effective manual teleoperation. The haptic interface contains a modified Delta parallel-link positioning mechanism. Parallel mechanisms are usually characterized by a high stiffness, which, however, is reduced by elastic deformations of both parts and bearings. Therefore, to design such a parallel mechanism, we should analyze its structural stiffness, including elastic deformations of both parts and bearings. Then we propose a simple method to analyze structural stiffness in a parallel mechanism using bearings. Our method is based on standard concepts such as static elastic deformations. However, the important aspect of our method is the manner in which we combine these concepts and how we obtain the value of the elasticity coefficient of a rotation axis in a bearing. Finally, we design a modified Delta mechanism, with a well-balanced stiffness, based on our method of stiffness analysis.

KEYWORDS: Design; Parallel mechanism; Modified Delta mechanism; Stiffness analysis; Bearing.

1. INTRODUCTION

In our previous work, in order to provide a high-quality teleoperation environment to an operator, a compact 6-DOF haptic interface was developed as a master arm of our teleoperation system.[1] The haptic interface, which is directly accessible to the operator, must be light, have a high stiffness and operate over a wide workspace. Thus, as positioning mechanism, we use a modified Delta mechanism, which is a kind of a parallel mechanism. Other parallel mechanisms (e.g. Stewart Platform,[2] Pantograph Linkage,[3] Delta,[4] HEXA[5]), which address the high stiffness of the tip position, have also been proposed. The modified Delta mechanism was originally proposed by Tsai in 1995,[6] however, the offset direction of the bearings of our modified Delta mechanism[1,7] is a little different from that of Tsai.

* Intelligent Systems Institute, National Institute of Advanced Industrial Science and Technology (AIST) 1-1-1 UMEZONO, TSUKUBA, 305-8568 (Japan).
† Department of Intelligent Machines and System Engineering, Hirosaki University (Japan).
‡ Department of Aeronautic and Space Engineering, Tohoku University (Japan).

In general, to realize a high stiffness mechanism, many parts should be large and heavy. However, to achieve a light and high speed motion, these should be small and light. Moreover, we should point out that the tip stiffness is greatly affected by both the positions and the values of the mechanical parameters of the structural parts, even if the mechanical structure is the same. Thus, to design a modified Delta mechanism with these characteristics, we need to analyze its stiffness including both elastic deformations and position of its parts.

So far, many researches on parallel mechanisms have been published, concerning motion analysis and singularity.[8–12] Svinin et al.[13] studied the static compliant motion of a serial manipulator with elastic deformations. The stiffness analysis of a parallel mechanism has been studied by Arai et al.[14] and Oiwa et al.[15]. Their studies did not include elastic deformations. Gosselin[16] also studied the stiffness for a parallel manipulator, however, his research considered only the stiffness of each actuator. Huang proposed a method of stiffness analysis for a parallel mechanism[17] that uses spherical bearings at the joints, unlike our modified Delta mechanism, which uses normal bearings (passive axis). Therefore, the method of Huang's analysis cannot apply to our modified Delta mechanism.

Thus, we propose a stiffness analysis method for parallel mechanisms, which takes into account elastic deformations of parts and bearings. Our analysis is based on tip position compliance and can be applied to many elastic deformations. Moreover, it uses the concept of the stiffness of a static flexible manipulator proposed by Komatsu.[18] The key points of our method are:

- a new method combining basic concepts on both static elastic deformation and parallel mechanism,
- a modeling of the value of the elasticity coefficient of a rotation axis in a bearing.

In order to design a modified Delta mechanism having a well-balanced tip stiffness, we apply our method of stiffness analysis for a parallel mechanism to the modified Delta mechanism and we derive the compliance matrix for this mechanism. In the following sections we discuss:

- the relation between a singular point and motion area,
- how each elastic deformation of both parts and bearings influences to the tip stiffness of the modified Delta mechanism,

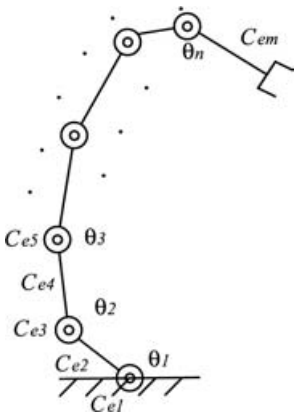

Fig. 1. Model of a serial manipulator.

- the realization of a well-balanced tip stiffness for the modified Delta mechanism,
- a design guideline for modified Delta mechanisms of various sizes.

Finally, we carry out stiffness analysis experiments in which we compare the stiffness of a real modified Delta mechanism built according to our design to that predicted by the analysis.

2. STIFFNESS ANALYSIS OF A PARALLEL MECHANISM

In this section, we present a method to analyze parallel mechanism stiffness including elastic deformations in the structure. First, we derive the compliance matrix for a serial manipulator; second, we derive the compliance matrix for a parallel manipulator using these results and third, we explain the modeling of the link and of the bearing.

2.1. Tip compliance of a serial manipulator

In this subsection, we derive the tip compliance matrix for a serial manipulator.[18] A serial manipulator consists of m elastically deformable elements and n joints, as shown in Fig. 1. Forces and moments elastically deform the positions and joints of each element and elastic deformations are written as follows:

$$e_i = [\delta_{xi} \quad \delta_{yi} \quad \delta_{zi} \quad \phi_{xi} \quad \phi_{yi} \quad \phi_{zi}]^T \tag{1}$$

where e_i is the elastic deformation vector of each element. δ_{xi}, δ_{yi} and δ_{zi} are the elastic linear deformations respectively. ϕ_{xi}, ϕ_{yi} and ϕ_{zi} are the elastic rotation deformations respectively.

e, the elastic deformation vector for all the elements is given by:

$$e = \begin{bmatrix} e_1^T & e_2^T & \cdots & e_n^T \end{bmatrix}^T. \tag{2}$$

Here, forces and moments act on each element. The elastic deformation vector at all the elements can be rewritten as follows:

$$e = C_e \begin{bmatrix} f_{l1}^T & f_{l2}^T & \cdots & f_{lm}^T \end{bmatrix}^T \tag{3}$$

$$C_e = \text{diag}\,[C_{e1} \quad C_{e2} \quad \cdots \quad C_{em}] \tag{4}$$

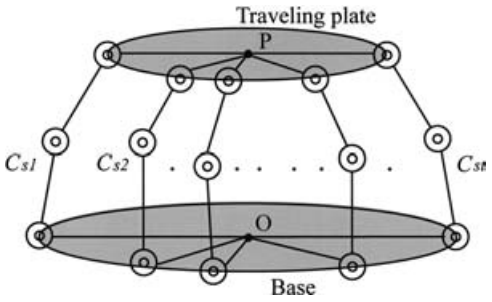

Fig. 2. Model of a parallel manipulator.

where C_e is the compliance matrix which is defined by the structural charcteristics of all the elements. C_{ei} is the local compliance matrix of each element. f_{li} are the forces and moments acting on each element.

C_s is the tip compliance matrix which is defined by the structural characteristics of all the elements and is given by

$$C_s = J_e(\theta, 0)\, C_e\, J_e^T(\theta, 0) \tag{5}$$

where θ is the joint angle vector. $J_e(\theta, e)$ are the jacobian matrices for each joint and each elastic deformation.

2.2. Tip compliance of a parallel manipulator

In this subsection, we derive the tip compliance matrix for a parallel manipulator using the compliance matrix of a serial manipulator presented in Section 2.1.

A model of parallel manipulator is shown in Fig. 2. This parallel manipulator consists of t serial manipulators. Point O is the origin and point P is the tip position of each serial manipulator. C_p, the tip compliance matrix of a serial manipulator is given by:

$$C_p^{-1} = C_{s1}^{-1} + C_{s2}^{-1} + \cdots + C_{st}^{-1} \tag{6}$$

where $C_{si}\,(i = 1, \cdots, t)$ is the compliance matrix of each serial manipulator. The elastic deformations of both traveling plate and base are ignored in this paper.

2.3. Modeling of the link

Forces and moments elastically deform the tip positions and joints of each link as shown in Fig. 3 and elastic deformations

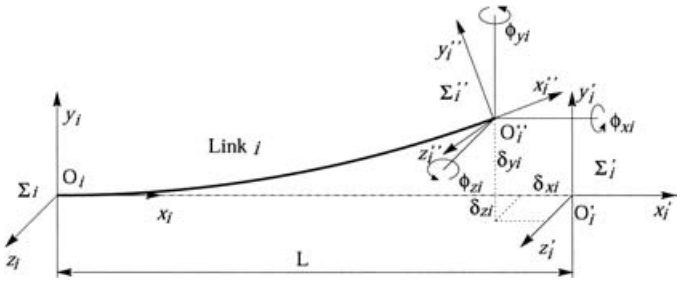

Fig. 3. Deformation at the tip of the link.

at the tip of the link are written as follows:

$$\begin{aligned}
\delta_{xi} &= \frac{L^3}{3EI_x}F_{xi} \\
\delta_{yi} &= \frac{L^3}{3EI_y}F_{yi} + \frac{L^2}{2EI_z}M_{zi} \\
\delta_{zi} &= \frac{L^3}{3EI_z}F_{zi} - \frac{L^2}{2EI_y}M_{yi} \\
\phi_{xi} &= \frac{L}{GI_p}M_{xi} \\
\phi_{yi} &= -\frac{L^2}{2EI_z}F_{zi} + \frac{L}{EI_y}M_{yi} \\
\phi_{zi} &= \frac{L^2}{2EI_y}F_{yi} + \frac{L}{EI_z}M_{zi}
\end{aligned} \tag{7}$$

where L is link length, E is the modulus of the longitudinal elasticity, G is the modulus of the transverse elasticity. I_x, I_y and I_z are the geometrical moment of inertias respectively. I_p is the polar moment of inertia. Then, C_{ei}, the compliance matrix of the link i is given by:

$$C_{ei} = \begin{bmatrix}
\frac{L^3}{3EI_x} & 0 & 0 & 0 & 0 & 0 \\
0 & \frac{L^3}{3EI_y} & 0 & 0 & 0 & -\frac{L^2}{2EI_z} \\
0 & 0 & \frac{L^3}{3EI_z} & 0 & \frac{L^2}{2EI_y} & 0 \\
0 & 0 & 0 & \frac{L}{GI_p} & 0 & 0 \\
0 & 0 & \frac{L^2}{2EI_z} & 0 & \frac{L}{EI_y} & 0 \\
0 & -\frac{L^2}{2EI_y} & 0 & 0 & 0 & \frac{L}{EI_z}
\end{bmatrix}. \tag{8}$$

2.4. Modeling of the bearing

C_{ei} is the compliance matrix of bearing i and is given by

$$C_{ei} = \begin{bmatrix}
\frac{1}{k_a} & 0 & 0 & 0 & 0 & 0 \\
0 & \frac{1}{k_r} & 0 & 0 & 0 & 0 \\
0 & 0 & \frac{1}{k_r} & 0 & 0 & 0 \\
0 & 0 & 0 & \Phi & 0 & 0 \\
0 & 0 & 0 & 0 & \frac{1}{k_m} & 0 \\
0 & 0 & 0 & 0 & 0 & \frac{1}{k_m}
\end{bmatrix} \tag{9}$$

where k_a is the coefficient of elasticity in the axial direction. k_r is the coefficient of elasticity in the radial direction. $\frac{1}{\Phi}$ is the coefficient of elasticity for axial rotation. k_m is the coefficient of elasticity for radial rotation. The direction of the x axis is chosen as the rotation axis.

If the rotation axis is passive, the coefficient of elasticity for axial rotation is almost zero and Φ is close to infinity. However, if Φ is chosen close to infinity, the numerical calculation becomes unstable. Therefore, for the numerical calculation to remain stable, Φ should not be chosen close to infinity. A detailed discussion of the effects of the value of Φ on the calculation is presented in Section 4.2.

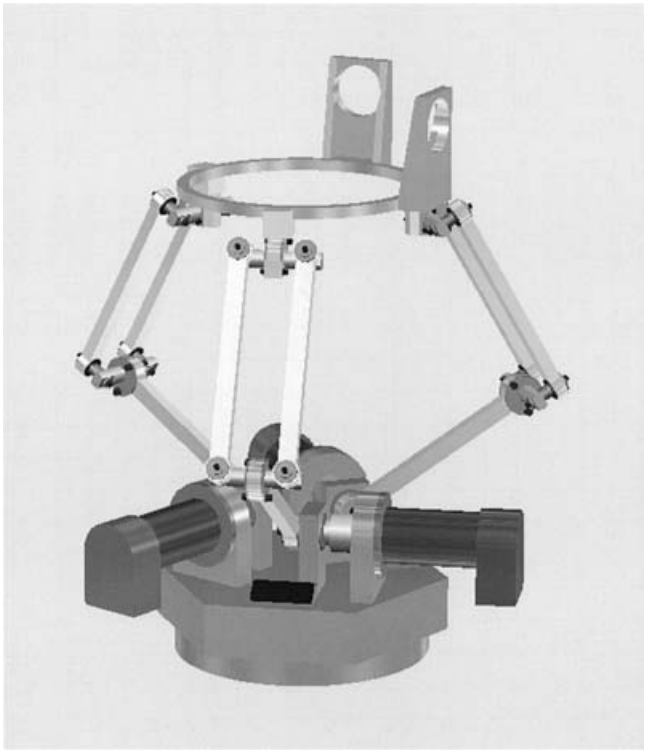

Fig. 4. Overview of the modified Delta mechanism.

3. COMPLIANCE MATRIX OF THE MODIFIED DELTA MECHANISM

In this section, we explain how to use our stiffness analysis method.

First, we describe the modified Delta mechanism to which our stiffness analysis is applied. Next, we explain the modeling of bearing pairs and the modeling of the modified Delta mechanism. Finally we derive the compliance matrix of the modified Delta mechanism.

3.1. The modified Delta mechanism

A overview of the modified Delta mechanism is shown in Fig. 4 and a schematic of this mechanism is shown in Fig. 5. This mechanism is made of a base, bearing 0, an arm, bearing 1, bearing 2, a rod, bearing 3, bearing 4 and a traveling plate. The rotation axis of the motor is inserted in bearing 0. The rod part which includes a planar parallel-link mechanism is made of bearing 2, two parallel rods and bearing 3. The passive joints are equipped with conventional bearings that are mounted in pairs (see Fig. 5).

3.2. Modeling of a pair of bearings

We now consider the compliance matrix for a pair of bearings mounted in parallel as shown in Fig. 6. The coefficients of elasticity in the axial and radial directions are multiplied by 2. The coefficient of elasticity for axial rotation is also multiplied by 2. However, the case of the coefficient of elasticity for radial rotation is different. The elastic deformation model of a pair of bearings is shown in

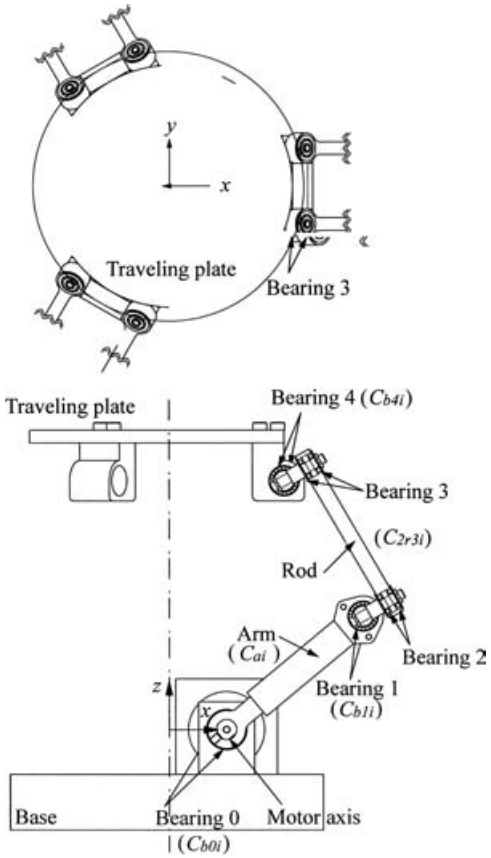

Fig. 5. Schematics of the modified Delta mechanism.

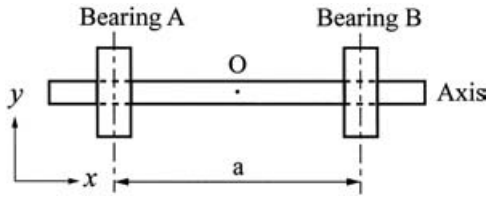

Fig. 6. Model of two bearings.

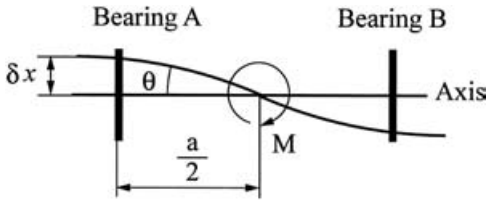

Fig. 7. Elastic deformation model of two bearings.

Fig. 7. δx is the elastic deformation in the radial direction. The moment M becomes

$$\begin{aligned} M &= 2\left(K_m\,\theta + \frac{a}{2}\delta x\,K_r\right) \\ &= 2\left(k_m\,\theta + \frac{a}{2}\frac{a}{2}\theta\,K_r\right) \\ &= 2\left(K_m + \left(\frac{a}{2}\right)^2 K_r\right)\theta. \end{aligned} \tag{10}$$

Therefore, the compliance matrix of the two bearings C_{ei} takes the following form:

$$C_{ei} = \begin{bmatrix} \frac{1}{2k_a} & 0 & 0 & 0 & 0 & 0 \\ 0 & \frac{1}{2k_r} & 0 & 0 & 0 & 0 \\ 0 & 0 & \frac{1}{2k_r} & 0 & 0 & 0 \\ 0 & 0 & 0 & \frac{\Phi}{2} & 0 & 0 \\ 0 & 0 & 0 & 0 & \frac{1}{2(k_m+(\frac{a}{2})^2 K_r)} & 0 \\ 0 & 0 & 0 & 0 & 0 & \frac{1}{2(k_m+(\frac{a}{2})^2 K_r)} \end{bmatrix}. \tag{11}$$

3.3. Modeling of the rod part with a parallel mechanism

We derive the compliance matrix of the rod part which is made of a planar parallel-link mechanism. This parallel-link mechanism is constituted by two parallel rods and bearings 2 and 3 as shown in Fig. 5. We consider separately the two rods (Rod L and R) as shown in Fig. 8 and calculate first the compliance matrix for each rod; the final matrix for the complete rod is calculated from these two matrices.

According to equation (4), the compliance matrices C_{eL} and C_{eR} as shown in Fig. 8, are given by

$$C_{eL} = \mathrm{diag}[C_{b2L}\,C_{rL}\,C_{b3L}] \tag{12}$$

and

$$C_{eR} = \mathrm{diag}[C_{b2R}\,C_{rR}\,C_{b3R}] \tag{13}$$

for rod L and R, respectively. Where C_{b2L}, C_{b2R}, C_{b3L} and C_{b3R} are the compliance matrices of bearing 2L, 2R, 3L and 3R, respectively. C_{rL} and C_{rR} are the compliance matrices of rod L and R, respectively.

$J_{eL}(\theta, 0)$ and $J_{eR}(\theta, 0)$ are written as

$$J_{eL}(\theta, 0) = [J_{b2L}(\theta, 0)\,J_{rL}(\theta, 0)\,J_{b3L}(\theta, 0)] \tag{14}$$

and

$$J_{eR}(\theta, 0) = [J_{b2R}(\theta, 0)\,J_{rR}(\theta, 0)\,J_{b3R}(\theta, 0)] \tag{15}$$

for rod L and R, respectively. Where $J_{b2L}(\theta, 0)$, $J_{b2R}(\theta, 0)$, $J_{b3L}(\theta, 0)$ and $J_{b3R}(\theta, 0)$ are the jacobian matrices of bearing 2L, 2R, 3L and 3R, respectively. $J_{rL}(\theta, 0)$ and $J_{rR}(\theta, 0)$ are the jacobian matrices of rod L and R, respectively.

The compliance matrices (C_{rodL} and C_{rodR}) of each part can be written as

$$C_{rodL} = J_{eL}(\theta, 0)\,C_{eL}\,J_{eL}^T(\theta, 0) \tag{16}$$

and

$$C_{rodR} = J_{eR}(\theta, 0)\,C_{eR}\,J_{eR}^T(\theta, 0) \tag{17}$$

for rod L and R, respectively. C_{2r3} is the compliance matrix of the rod part and can be written as

$$C_{2r3}^{-1} = C_{rodL}^{-1} + C_{rodR}^{-1}. \tag{18}$$

3.4. Modeling of the modified Delta mechanism

In this subsection, we derive the compliance matrix of the modified Delta mechanism.

The modified Delta mechanism consists of three arms, as shown in Fig. 4. Each serial manipulator is connected to the same traveling plate which does not deform elastically.

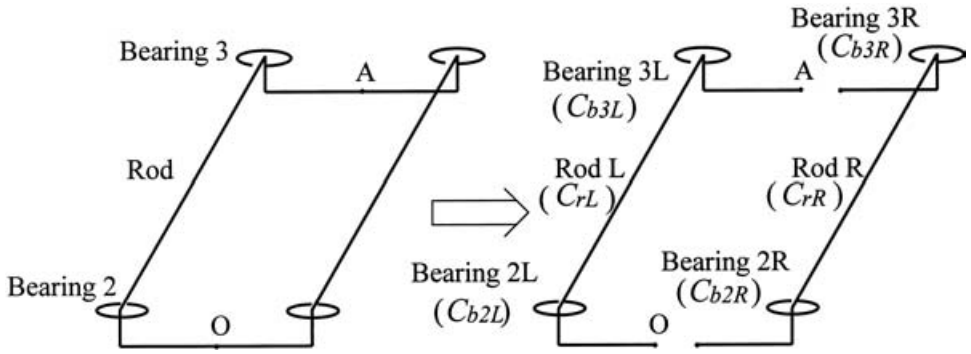

Fig. 8. Modeling of the rod part.

Moreover, a position on the traveling plate corresponds to a common tip position for the three serial manipulators.

We first derive the compliance matrix for a single serial manipulator, which consists of the base, one arm, one rod part, bearings 0, 1, 4 and the traveling plate (see Fig. 5). Then, the compliance matrices of the three arms are combined to obtain that of the modified Delta mechanism.

C_{eSi} (i = 1, 2, 3) of three serial manipulator given in equation (4) is rewritten as

$$C_{eSi} = \text{diag}[C_{b0i}\ C_{ai}\ C_{bli}\ C_{2r3i}\ C_{b4i}] \tag{19}$$

where C_{b0i}, C_{b1i} and C_{b4i} are the compliance matrices of bearing 0, 1, and 4 respectively. C_{ai} is the compliance matrix of the arm. C_{2r3i} is the compliance matrix of the rod part.

$J_{eSi}(\theta, 0)$ can be rewritten as

$$J_{eSi}(\theta, 0) = [J_{b0i}(\theta, 0)\, J_{ai}(\theta, 0)\, J_{b1i}(\theta, 0)\, J_{2r3i}(\theta, 0) \times J_{b4i}(\theta, 0)] \tag{20}$$

where $J_{b0i}(\theta, 0)$, $J_{b1i}(\theta, 0)$ and $J_{b4i}(\theta, 0)$ are the jacobian matrices of bearings 0, 1 and 4 respectively. $J_{ai}(\theta, 0)$ is the jacobian matrix of the arm. $J_{2r3i}(\theta, 0)$ is the jacobian matrix of the rod part.

C_{si} is the compliance matrix of each serial manipulator and is written as

$$C_{si} = J_{eSi}(\theta, 0)\, C_{esi}\, J_{eSi}^{T}(\theta, 0). \tag{21}$$

We consider the modified Delta mechanism as made of three serial manipulators and thus compliance matrix C_p can be written as:

$$C_p^{-1} = C_{s1}^{-1} + C_{s2}^{-1} + C_{s3}^{-1}. \tag{22}$$

4. PARAMETERS OF THE MODIFIED DELTA MECHANISM

In this section, we define the parameters of the parts which form the modified Delta mechanism. In order to carry out a numerical calculation based on our stiffness analysis, we discuss the modeling of the value of the elasticity coefficient of a rotation axis in a bearing. Finally, we calculate the tip compliance matrix value of the modified Delta mechanism.

4.1. Parameters of the parts of the mechanism

A schematic of the modified Delta mechanism identifying the parameters is shown in Fig. 9. Point O is the origin and point T is the tip position. L is the arm length, M is the rod length, R is the base radius, r is the traveling plate radius and z is the traveling plate height which is the distance between points O and S. Here, the distance between points S and T is 15.0 mm and the distance between the two parallel rods which form the rod part is 31.0 mm.

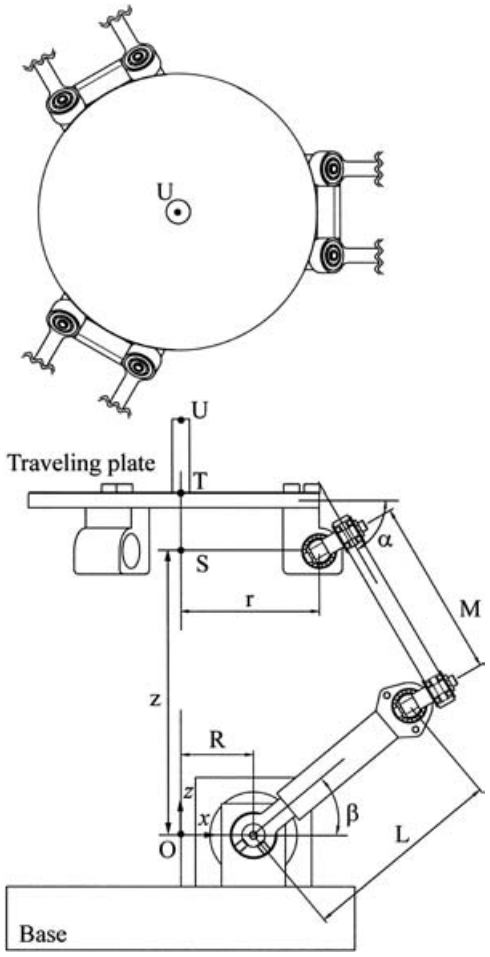

Fig. 9. Schematics of the modified Delta mechanism for parameters.

The value of the fixed parameters of the modified Delta mechanism are given in Table I. More specific details on the parts of the modified Delta mechanism are given below.

- The arm is a hollow pole, made of A7075 material, with an internal diameter of 8 mm and an external diameter of 12 mm.
- The rod is a prismatic beam, made of SUS304 material, one side measure 5 mm and another side measure 6 mm.

Table I. Base parameters of the modified Delta mechanism.

Parameter	[mm]
M (Rod length)	110.0
L (Arm length)	110.0
R (Radius of base)	40.0
r (Radius of traveling plate)	40.0

- Bearing 0 is a model F688A made by NSK.
- Bearing 1 and 4 are models MR128 made by NSK.
- Bearing 2 and 3 are models F684 made by NSK.
- The motor is a model A-max 26 (11 W) made by Maxon.

All bearings are used in pairs. From the values of Table I and the characteristics of the above parts, we calculate the compliance matrix of each part.

For the linear parts, we set the x direction axis along the length direction of the arm, of the rod R and L. The rotation axis is defined as the x axis direction for bearings 0, 1, 2, 3 and 4. All the elastic deformation data of the bearings are obtained from NSK. Here, we should take into account the value of Φ for bearing 0 since the rotation axis of the motor is inserted into this bearing. The compliance of this rotation axis might depend on the performance of the motor, the control rule, etc. Therefore we got the value of 0.0058 rad/Nm for this axis measured directly in real conditions of movement.

The compliance matrix of the arm defined in equation (8) is written as

$$C_{ai} = \begin{bmatrix} 0.0050 \times 10^{-6} & 0.0 & 0.0 & 0.0 & 0.0 & 0.0 \\ 0.0 & 4.4176 \times 10^{-6} & 0.0 & 0.0 & 0.0 & 60.2 \times 10^{-6} \\ 0.0 & 0.0 & 4.4176 \times 10^{-6} & 0.0 & -60.2 \times 10^{-6} & 0.0 \\ 0.0 & 0.0 & 0.0 & 0.0014 & 0.0 & 0.0 \\ 0.0 & 0.0 & -60.2 \times 10^{-6} & 0.0 & 0.0010 & 0.0 \\ 0.0 & 60.2 \times 10^{-6} & 0.0 & 0.0 & 0.0 & 0.0010 \end{bmatrix}.$$

The compliance matrix of rods L and R defined in equation (8) are written as

$$C_{rL} = C_{rR} = \begin{bmatrix} 26.4607 \times 10^{-6} & 0.0 & 0.0 & 0.0 & -0.0003608 & 0.0 \\ 0.0 & 38.1034 \times 10^{-6} & 0.0 & 0.0005195 & 0.0 & 0.0 \\ 0.0 & 0.0 & 0.0196 \times 10^{-6} & 0.0 & 0.0 & 0.0 \\ 0.0 & 0.0003608 & 0.0 & 0.0094 & 0.0 & 0.0 \\ -0.0005195 & 0.0 & 0.0 & 0.0 & 0.0065 & 0.0 \\ 0.0 & 0.0 & 0.0 & 0.0 & 0.0 & 0.0126 \end{bmatrix}.$$

The compliance matrix of bearing 0 defined in equation (11) is written as

$$C_{b0i} = \begin{bmatrix} 0.4081 \times 10^{-6} & 0.0 & 0.0 & 0.0 & 0.0 & 0.0 \\ 0.0 & 0.0892 \times 10^{-6} & 0.0 & 0.0 & 0.0 & 0.0 \\ 0.0 & 0.0 & 0.0892 \times 10^{-6} & 0.0 & 0.0 & 0.0 \\ 0.0 & 0.0 & 0.0 & 0.0058 & 0.0 & 0.0 \\ 0.0 & 0.0 & 0.0 & 0.0 & 0.0006 & 0.0 \\ 0.0 & 0.0 & 0.0 & 0.0 & 0.0 & 0.0006 \end{bmatrix}.$$

The compliance matrix of bearings 1 and 4 defined in equation (11) are written as

$$C_{b1i} = C_{b4i} = \begin{bmatrix} 0.2551 \times 10^{-6} & 0.0 & 0.0 & 0.0 & 0.0 & 0.0 \\ 0.0 & 0.0918 \times 10^{-6} & 0.0 & 0.0 & 0.0 & 0.0 \\ 0.0 & 0.0 & 0.0918 \times 10^{-6} & 0.0 & 0.0 & 0.0 \\ 0.0 & 0.0 & 0.0 & \Phi/2 & 0.0 & 0.0 \\ 0.0 & 0.0 & 0.0 & 0.0 & 0.0003 & 0.0 \\ 0.0 & 0.0 & 0.0 & 0.0 & 0.0 & 0.0003 \end{bmatrix}.$$

The compliance matrix of bearings 2L, 2R, 3L and 3R defined in equation (11) are written as

$$C_{b2L} = C_{b2R} = C_{b3L} = C_{b3R} = \begin{bmatrix} 0.4081 \times 10^{-6} & 0.0 & 0.0 & 0.0 & 0.0 & 0.0 \\ 0.0 & 0.1020 \times 10^{-6} & 0.0 & 0.0 & 0.0 & 0.0 \\ 0.0 & 0.0 & 0.1020 \times 10^{-6} & 0.0 & 0.0 & 0.0 \\ 0.0 & 0.0 & 0.0 & \Phi/2 & 0.0 & 0.0 \\ 0.0 & 0.0 & 0.0 & 0.0 & 0.0254 & 0.0 \\ 0.0 & 0.0 & 0.0 & 0.0 & 0.0 & 0.0254 \end{bmatrix}.$$

The units of these compliance matrix elements are as follows:

$$\begin{bmatrix} \text{m/N} & \text{m/N} & \text{m/N} & \text{1/N} & \text{1/N} & \text{1/N} \\ \text{m/N} & \text{m/N} & \text{m/N} & \text{1/N} & \text{1/N} & \text{1/N} \\ \text{m/N} & \text{m/N} & \text{m/N} & \text{1/N} & \text{1/N} & \text{1/N} \\ \text{rad/N} & \text{rad/N} & \text{rad/N} & \text{rad/Nm} & \text{rad/Nm} & \text{rad/Nm} \\ \text{rad/N} & \text{rad/N} & \text{rad/N} & \text{rad/Nm} & \text{rad/Nm} & \text{rad/Nm} \\ \text{rad/N} & \text{rad/N} & \text{rad/N} & \text{rad/Nm} & \text{rad/Nm} & \text{rad/Nm} \end{bmatrix}.$$

4.2. Elastic coefficient of a rotation axis in a bearing

If a bearing is used in a passive axis joints, Φ (the value of the passive axis compliance) is close to infinity. However if Φ is chosen close to infinity, the numerical calculation becomes unstable. Therefore, for the numerical calculation to remain stable, Φ should not be chosen close to infinity.

When Φ is changed from zero to infinity, the passive axis condition of the bearing is changed from rigid to passive. Since to be able to carry out our analysis, the calculation must remain stable, we must choose a value for Φ that dose not perturb the calculation but that is much higher than any other matrix element. We will address this question in the next paragraphs.

The tip of the traveling plate is locked at one position, whose height (z) is 135.0 mm, in the z axis direction, as shown in Fig. 9. Figure 10 shows the elements of the tip compliance matrix (C_p) Curves A to F in the Figure correspond to the following matrix elements:

$$C_p = \begin{bmatrix} \text{A} & 0.0 & 0.0 & 0.0 & \text{B} & 0.0 \\ 0.0 & \text{A} & 0.0 & -\text{B} & 0.0 & 0.0 \\ 0.0 & 0.0 & \text{C} & 0.0 & 0.0 & 0.0 \\ 0.0 & -\text{B} & 0.0 & \text{D} & 0.0 & 0.0 \\ \text{B} & 0.0 & 0.0 & 0.0 & \text{D} & 0.0 \\ 0.0 & 0.0 & 0.0 & 0.0 & 0.0 & \text{E} \end{bmatrix}. \quad (23)$$

Here the tip compliance matrix (equation (23)) is very simple because the tip position is set along the z axis direction.

All the matrix elements display two regions of stability and one region of unstability as a function of Φ: the first stable region for $\Phi < 10^{-4}$, the second one for $10 < \Phi$ and the unstable region for $10^{-4} < \Phi < 10$.

The first stable region ($\Phi < 10^{-4}$) corresponds to a rigid axis (Φ is almost zero) whereas the second one ($10 < \Phi$) corresponds to a passive axis (Φ is almost infinity). The unstable region ($10^{-4} < \Phi < 10$) corresponds to an elastic axis. Here we should notice that the numerical calculation becomes unstable when the value of Φ is smaller than 10^{-10} and larger than 10^{10}. Based on these results, a value of 10^8 rad/Nm is used for Φ in this paper, which is much larger than any other matrix element and is in the stable region for a numerical calculation. This value of Φ clearly reflects that of a bearing passive axis.

4.3. Tip compliance matrix of the modified Delta mechanism

We can now calculate the tip compliance matrix of the modified Delta mechanism using the parameters given in Sections 4.1 and 4.2.

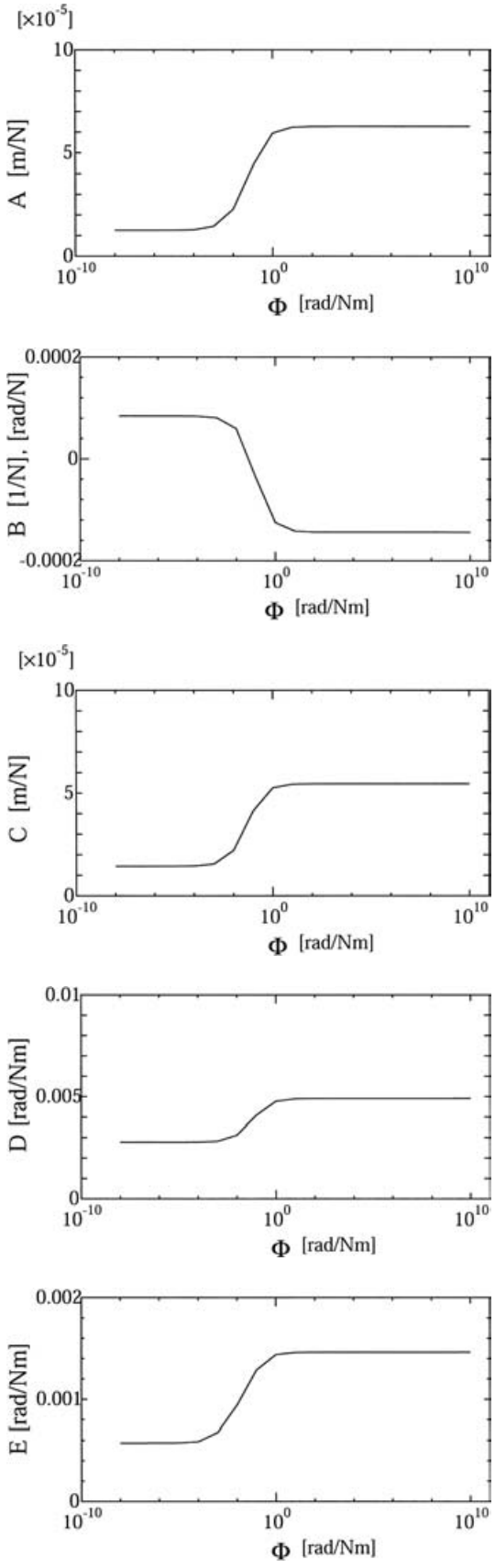

Fig. 10. Calculation results.

The tip of the traveling plate is locked at one position, whose height (z) is 135.0 mm, in the z axis direction, as shown in Fig. 9. Under these conditions, the tip compliance

matrix is calculated as follows:

$$C_p = \begin{bmatrix} 0.000087 & 0.0 & 0.0 & 0.0 & -0.000094 & 0.0 \\ 0.0 & 0.000087 & 0.0 & 0.000094 & 0.0 & 0.0 \\ 0.0 & 0.0 & 0.000032 & 0.0 & 0.0 & 0.0 \\ 0.0 & 0.000094 & 0.0 & 0.003133 & 0.0 & 0.0 \\ -0.000094 & 0.0 & 0.0 & 0.0 & 0.003133 & 0.0 \\ 0.0 & 0.0 & 0.0 & 0.0 & 0.0 & 0.001912 \end{bmatrix}.$$

5. DESIGN OF A MODIFIED DELTA MECHANISM BASED ON OUR STIFFNESS ANALYSIS

Several different methods could be used to transfer the results of our numerical analysis into the mechanical design of modified Delta mechanism with a well-balanced tip stiffness. We have adopted the following sequence:

(i) We first consider the relation between the singular point and motion area.
(ii) We identify the parts having a large influence on the reduction of tip stiffness.
(iii) We discuss how each elastic deformation of both parts and bearings influences the tip stiffness of the modified Delta mechanism.
(iv) We discuss the parameters that are important to realize a well-balanced tip stiffness.
(v) Finally, we propose a design guideline common to modified Delta mechanism of various sizes and design a new modified Delta mechanism.

5.1. Singular point and motion area in a Delta mechanism

A singular point called the under mobility and the over mobility within the motion area exists in parallel mechanisms,[19] such as HEXA and Delta mechanisms. Tsumaki et al. discussed the relation between singular point and motion area in the modified Delta mechanism,[7] and based on their results, we chose to make the base radius and the traveling plate radius identical in our design.

5.2. Influence on the tip stiffness from the stiffness of each part

In the following discussion, since the motion area is set as a sphere of 75 mm radius, we set the sum of the arm length and of the rod length to 220 mm, and the minimum height to 50 mm in order to avoid the under mobility, and the maximum height to 200 mm in order to avoid the over mobility. According to Section 5.1, the traveling plate radius and the base radius are both set to 40 mm. Point O is the origin and point U is the tip position. Here, the distance between points S and T is 15.0 mm and the distance between point T and U is 63.5 mm.

In this paper, it is assumed that the arms, rods, motor axes, bearings 0, 1, 2, 3 and 4 deform elastically.

The stiffness of the tip position (point U, see Fig. 9) of the modified Delta mechanism changes strongly with the position of a traveling plate. Therefore, it is necessary to design the mechanism taking into consideration the tip stiffness in all the positions of the motion area. However, the evaluation method becomes complicated and it is very difficult to evaluate all the elements (36 pieces) of the tip compliance matrix at many points. In this paper, we simplify the evaluation by considering only movements in the z direction, with no movement of the traveling plate in the (x, y) plane. Thus, the effect on the tip stiffness of moving the height of the traveling plate from $z = 50$ mm to 200 mm along the z axis is evaluated.

5.2.1. Influence on the tip stiffness from the each individual part. We first assume that each part deforms elastically individually. For instance, we consider that only the arm deforms elastically while other parts do not deform. From this study, we will be able to find the part the stiffness of which has a large influence on the tip stiffness.

The changes of the elements of the tip compliance matrix (C_p) due to individual elastic deformation of each part using the base parameters are shown in Fig. 11.

In this Figure, all the matrix elements are plotted as a function of α which is the joint between the rod and the traveling plate. The reason for this choice is that α will be one of the major elements of the design guideline of the modified Delta mechanism as shown by the following arguments. Curves A to E in the Figure correspond to equation (23). Here we can evaluate the stiffness easily since the tip compliance matrix (equation (23)) becomes very simple.

According to Fig. 11, the stiffness of bearings 0, 2, and 3 affects the tip stiffness mostly through elements A and B of the compliance matrices, and the stiffness of the arm affects the tip stiffness mostly through elements C, D and E.

The stiffness of the rotation axis of the motor is included in the stiffness of bearing 0, and this stiffness increases the value of elements A and B. Althoug these elements can be decreased by the stiffness of the rotation axis of the motor and by a change of the motor control, we do not consider such a change of the motor and the control in this paper. Therefore, we do not consider this stiffness in the following arguments.

From the above results, the influence on elements A and B of bearings 2 and 3 can be decreased by changing F648 steel bearings to F684 ceramic bearings. The influence on elements C, D and E of the arm can be decreased by increasing the arm radius.

5.2.2. Influence on the tip stiffness from the stiffness of all the parts together. The changes of the compliance matrix for the tip position (point U) under elastic deformation of all the components together (arms, rods, motor axes, bearings 0, 1, 2, 3, and 4) using the base parameters are shown in Fig. 12. In these calculations, F684 ceramic bearings are used for bearings 2 and 3 based on the results of Section 5.2.1. And we set the arm internal diameter to 10 mm and its external diameter to 14 mm.

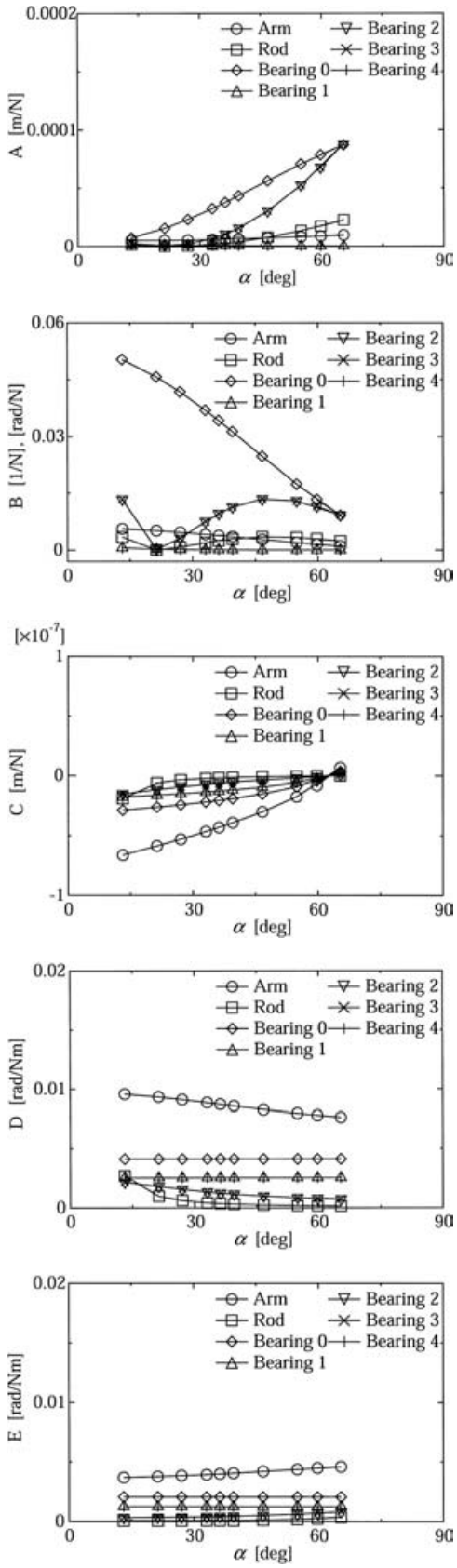

Fig. 11. Factors of compliance matrices.

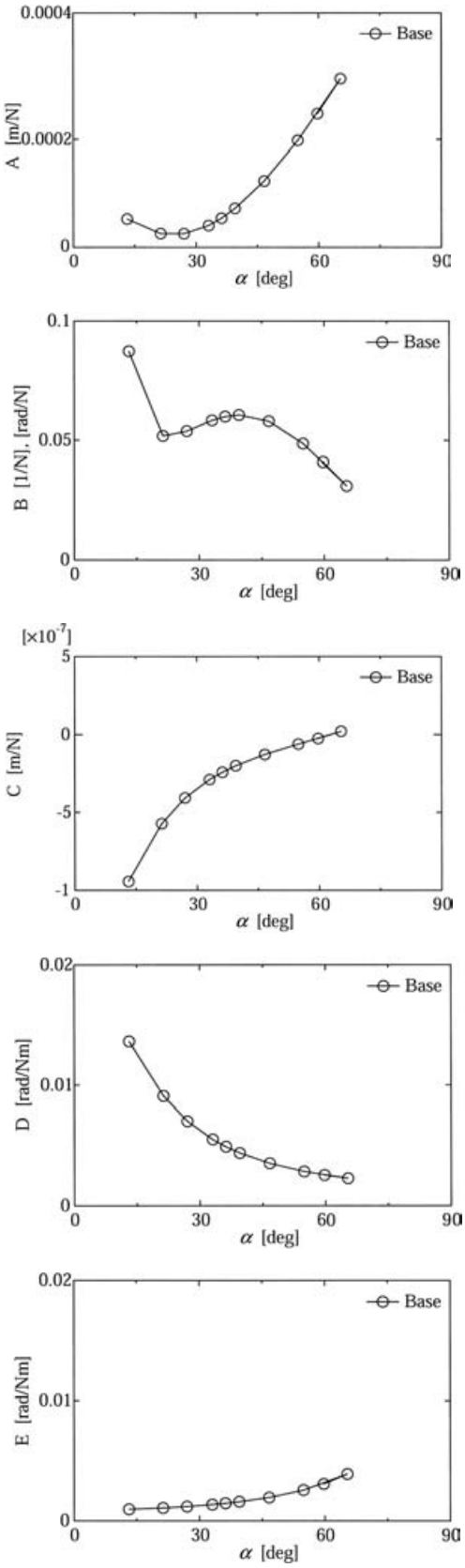

Fig. 12. Factors of a compliance matrix including all elastic deformations.

According to Fig. 12, when α increases, each of these elements changes as follows.

- The stiffness (element A) of both x and y axis directions decreases due to the force.
- The stiffness (element B) of both x and y rotation axes increases due to the force.
- The stiffness (element C) of z axis direction increases due to the force.

Table II. Parameters of two modified Delta mechanisms.

Parameter [mm]	Type 1	Type 2
M (Rod length)	120.0	130.0
L (Arm length)	100.0	90.0
R (Radius of base)	40.0	40.0
r (Radius of traveling plate)	40.0	40.0

- The stiffness (element B) of both x and y axis directions increases for the most part due to the moment, although it decreases for a while at about 50 degrees.
- The stiffness (element D) of both x and y rotation axes increases due to the moment.
- The stiffness (element E) of z rotation axis decreases due to the moment.

These tendencies of stiffness change were also observed in an experiment which used the real modified Delta mechanism.[7] As α becomes large, the stiffness of each element increases or decreases. Therefore, in order to obtain a well-balanced stiffness against both the force and the moment, it is necessary to limit the value that α can take within the motion area.

Here, if the value of β in Fig. 12 is positive within the motion area, even if the ratio of the base radius to the traveling plate radius changes and the stiffness of each part changes, the graph of Fig. 12 shows the same tendency. We conclude therefore from the above results that α becomes a major element of the design guideline of a general modified Delta mechanism.

From the above discussion, we may set α as a design guideline element while β is not set up as a design guideline element in this paper. Here, we should notice that the value of α depends on the base radius, the traveling plate radius, the arm length and the rod length.

5.2.3. Relation between tip stiffness and α. We will discuss how the tip stiffness change of the modified Delta mechanism depends on the value of α which is the joint between the rod and the traveling plate.

If the arm length is shortened, the rod length should be lengthened to keep the same full motion area and the value of α becomes large in this case. To study the change of tip stiffness under changes of arm length and rod length, we repeat the calculations with two other values of the parameters corresponding to the arm and rod lengths as shown in Table II. Fig. 13 compares the effect on tip stiffness of the elastic deformation of all the parts, using the base parameters (Table I) and the parameters of Table II.

According to Fig. 13, we see that the set of parameters labeled Type 2 in Table II provide the highest stiffness in all elements except for element E. A value of α in the range from 40 to 70 degrees is the best range for realizing a well-balanced tip stiffness. If the value of α is outside this range, the stiffness of many elements decreases. Therefore, we can conclude that Type 2 parameters form the better-balanced set of parameters. Here, we note that the variation of C, D and E with α does not depend on the set of parameters (Base, Type 1 or Type 2) and it is easy to calculate. If the tip position (point U) is set on point S, the variation of A and B does not depend either on the set of parameters (Base, Type 1 or Type 2) like C, D and E.

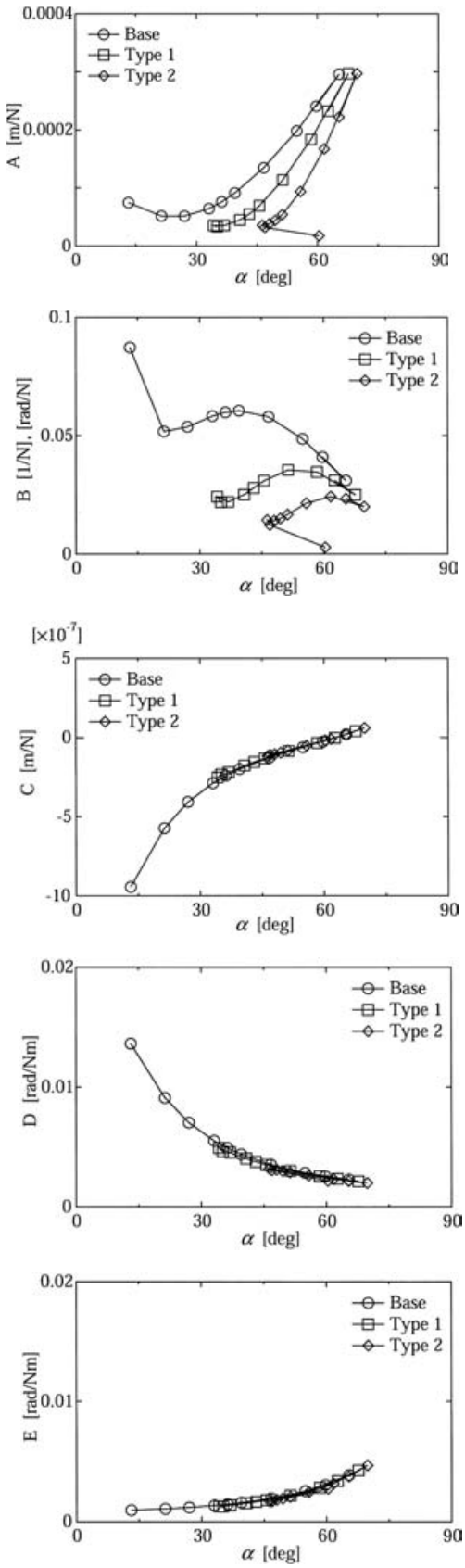

Fig. 13. Factors of compliance matrices.

In general, when z increases, α also increases. However, when z is between 50 mm and 94 mm, α becomes negative

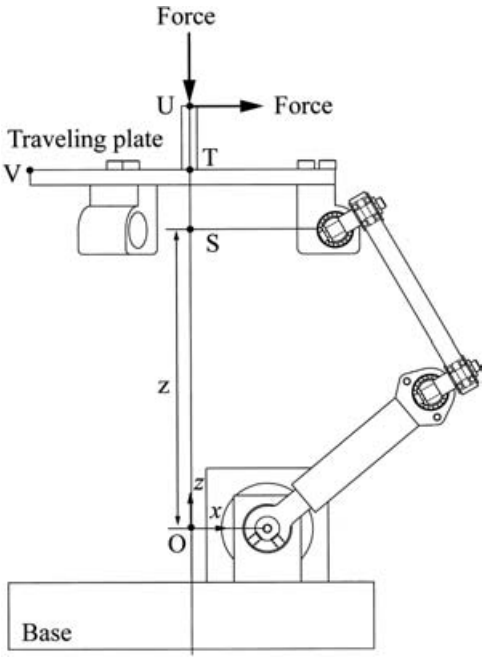

Fig. 14. Schematics of the modified Delta mechanism for the experiment.

and α decreases in the Type 2 case. Therefore, the curves for elements A and B in the Type 2 case are different from the other curves.

From the above results, the tip stiffness of the modified Delta mechanism is changed widely even if many parameters are not changed. It is important to limit the value of α within the motion area. Then we can conclude that to obtain a well-balanced tip stiffness in the modified Delta mechanism studied in this paper, the parameters should be chosen such that α is in the range from about 40 to 70 degrees. Therefore, we will decide that the traveling plate and the base radii are 40 mm, the arm length is 93 mm and the rod length is 127 mm in order to obtain the desired motion area (a sphere of about 150 mm diameter).

6. COMPARISON WITH THE STIFFNESS OF THE MODIFIED DELTA MECHANISM

We compare the stiffness of the modified Delta mechanism developed from the results of Section 5 to that predicted by the analysis. In this experiment, we calculate the elastic deformation of the tip position using our stiffness analysis method when we apply a force or a moment at the tip position. And we compare the result of our numerical calculation to the result of the real modified Delta mechanism.

Fig. 14 shows the schematics of the modified Delta mechanism for the experiment. All the parts are the same as in the previous sections and the parameters are those chosen in Section 5.2.3, and given in Table III. Here, point O is the origin and point U is the tip position. The distance between points S and T is 15.0 mm, the distance between point T and U (D_{tu}) is 78.0 mm and the distance between points T and V (D_{tv}) is 64.5 mm.

The force and the moment at point U (F_u), the elastic deformation vector of point T (e_t) and the elastic deformation vector of point V (e_v) are written as follows:

Table III. Parameters of the modified Delta mechanism.

Parameter	[mm]
M (Rod length)	127.0
L (Arm length)	93.0
R (Radius of base)	40.0
r (Radius of traveling plate)	40.0

$$F_u = [f_{xu} \quad f_{yu} \quad f_{zu} \quad m_{xu} \quad m_{yu} \quad m_{zu}]^T \tag{24}$$

$$e_t = [\delta_{xt} \quad \delta_{yt} \quad \delta_{zt} \quad \phi_{xt} \quad \phi_{yt} \quad \phi_{zt}]^T \tag{25}$$

$$e_v = [\delta_{xv} \quad \delta_{yv} \quad \delta_{zv} \quad \phi_{xv} \quad \phi_{yv} \quad \phi_{zv}]^T \tag{26}$$

where f_{xu}, f_{yu}, f_{zu}, m_{xu}, m_{yu} and m_{zu} are the forces and moments of each axis direction and each axis rotation for point U, respectively. δ_{xt}, δ_{yt}, δ_{zt}, ϕ_{xt}, ϕ_{yt} and ϕ_{zt} are the elastic deformations of each axis direction and each axis rotation of point T. δ_{xv}, δ_{yv}, δ_{zv}, ϕ_{xv}, ϕ_{yv} and ϕ_{zv} are the elastic deformations of each axis direction and each axis rotation of point V.

From these equations and equation (22) which is the tip compliance matrix (C_p), e_t can be written as follows:

$$e_t = C_p \, F_u. \tag{27}$$

And the relation between point T and V is written as

$$\begin{aligned} \delta_{xv} &= \delta xt + D_{tv}(1 - \cos\phi_{yt}) \\ \delta_{yv} &= \delta yt \\ \delta_{zv} &= \delta zt + \sin\phi_{yt} \, D_{tv} \\ \phi_{xv} &= \phi xt \\ \phi_{yv} &= \phi yt \\ \phi_{zv} &= \phi zt. \end{aligned} \tag{28}$$

The experiment is executed in two steps, as follows. In experiment (1) we apply a transverse force ($F_x = 4.9$ N) to the tip position (point U) in the x direction in the servo and in experiment (2) we apply a transverse force ($F_z = 4.9$ N) to the tip position (point U) in the z direction in the servo. In each case, a force and a moment are generated on point T. This experiment is repeated for different values of z along the vertical direction. The tip stiffness (C_p) changes with the height of the traveling plate. We can then compare the calculated values of the elastic deformation at point V to the values obtained for the real modified Delta mechanism. The numerical analysis with the conditions of experiment (1), shows that the elastic deformations are:

$$\delta_{yt} = \phi_{xt} = \phi_{zt} = 0 \tag{29}$$

and

$$\delta_{yv} = \phi_{xv} = \phi_{zv} = 0. \tag{30}$$

Thus, in experiment (1) we only compare δ_{xv} and δ_{zv}.

Similarly, in experiment (2), the calculated elastic deformations are:

$$\delta_{xt} = \delta_{yt} = \phi_{xt} = \phi_{yt} = \phi_{zt} = 0 \tag{31}$$

and

$$\delta_{xv} = \delta_{yv} = \phi_{xv} = \phi_{yv} = \phi_{zv} = 0. \tag{32}$$

Thus, in experiment (2) we only compare δ_{zv}.

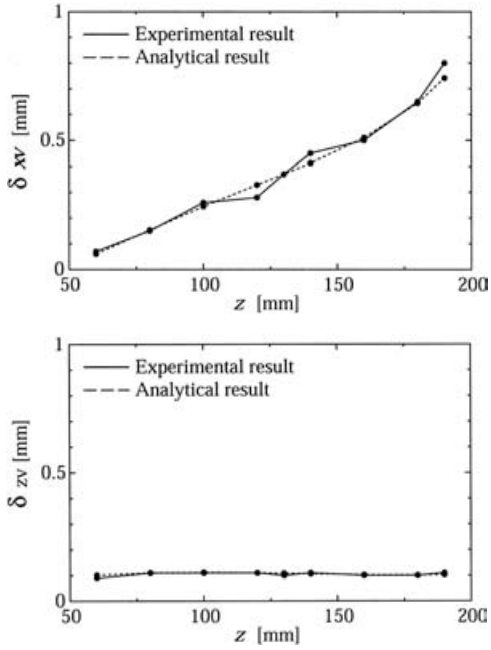

Fig. 15. Experiment 1.

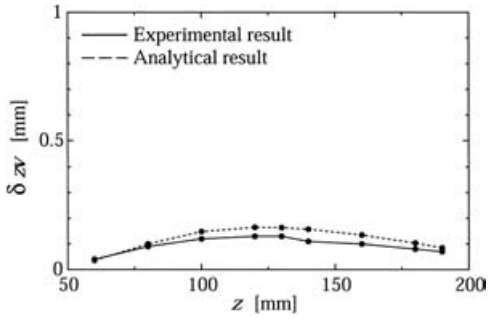

Fig. 16. Experiment 2.

Figures 15 and 16 show the results of experiments (1) and (2), respectively. The horizontal axis is the height (between point O and S) of the traveling plate and the vertical axis is the elastic deformation. These Figures show that the stiffness change of the real modified Delta mechanism is predicted by the numerical analysis. The irregular variation of the experimental values observed in the Figures seems to be most likely due to measurements errors and etc in the real mechanism. From above results, we can conclude that we have successfully built a modified Delta mechanism which has a well-balanced stiffness.

7. CONCLUSION

In this paper, we proposed a stiffness analysis method for a parallel mechanism, which takes into account elastic deformations in the structure. This method is based on the tip compliance of the link, and can be applied to both serial and parallel mechanisms. The key points of our method are:

- a new method combining basic ideas on both static elastic deformation and parallel mechanism,
- a modeling of the value of the elasticity coefficient of a rotation axis in a bearing.

Our method was applied to the compact 6-DOF haptic interface that has been developed in our laboratory and which includes a modified Delta parallel-link mechanism. We obtained the following results.

- The stiffness of bearing 2 and 3 is insufficient.
- α will be the design guideline parameter to evaluate the stiffness of the modified Delta mechanism.

From these results, we proposed that α is restricted to values from 40 to 70 degrees in order to obtain a well-balanced stiffness in each axial direction and rotation. Moreover, we set the base radius and the traveling plate radius to 40 mm, the arm length to 93 mm and the rod length to 127 mm in order to increase the tip stiffness and maintain a motion area to a sphere of about 150 mm diameter.

The experiment showed that the modified Delta mechanism has a sufficient stiffness as expected from the analysis. Therefore, we have been able to develop a modified Delta mechanism with a well-balanced tip stiffness.

References

1. Y. Tsumaki, H. Naruse, D. N. Nenchev and M. Uchiyama, "Design of a Compact 6-DOF Haptic Interface," *Proc. of the 1998 IEEE Int. Conf. on Robotics and Automation* (1998) pp. 2580–2585.
2. D. Stewart, "A Platform with Six Degrees of Freedom," *Proc. of the Institution of Mechanical Engineers 1965–1966* **180**(15), Part 1, 371–386 (1965).
3. H. Inoue, Y. Tsusaka and T. Fukuizumi, "Parallel Manipulator," *Robotics Research, The Third Int. Symposium* (O. Faugeras and G. Giralt Eds.) (The MIT Press), (1986) pp. 321–327.
4. R. Clavel, "DELTA, a fast robot with parallel geometry," *Proc. Int. Symposium on Industrial Robots* (1988) pp. 91–100.
5. F. Pierrot, M. Uchiyama, P. Dauchez and A. Fournier, "A New Design of a 6-DOF Parallel Robot," *J. Robotics and Mechatronics* **2**(4), 308–315 (1991).
6. L. W. Tsai, "Multi-degree-of-freedom mechanisms for machine tools and the like," *U. S. Patent Pending*, No. 08/415, 851 (1995).
7. H. Inou, Y. Tsumaki and M. Uchiyama, "Improvement of a Compact 6-DOF Haptic Interface," *Proc. of 2002 JSME Conference on Robotics and Mechatronics, 2P1-E02* (2002) (in Japanese).
8. R. E. Stamper, L. W. Tsai and G. C. Walsh, "Optimization of a Three DOF Translational Platform for Well-Conditioned Workspace," *Proc. of the 1997 IEEE Int. Conf. on Robotics and Automation* (1997) pp. 3250–3255.
9. L. Baron and J. Angeles, "The Direct Kinematics of Parallel Manipulators Under Joint-Sensor Redundancy," *IEEE Transactions on Robotics and Automation* **16**(1), 12–19 (2000).
10. M. J. Liu, C. X. Li and C. N. Li, "Dynamics Analysis of the Gough-Stewart Platform Manipulator," *IEEE Transactions on Robotics and Automation* **16**(1), 94–99 (2000).
11. J. E. McInroy and J. C. Hamann, "Design and Control of Flexure Jointed Hexapods," *IEEE Transactions on Robotics and Automation* **16**(4), 372–381 (2000).
12. X. J. Liu, J. Wang, F. Gao and L. P. Wang, "Mechanism design of a simplified 6-DOF 6-RUS parallel manipulator," *Robotica* **20**(1), 81–91 (2002).
13. M. M. Svinin and M. Uchiyama, "Contribution to Inverse Kinematics of Flexible Robot Arms," *JSME International J. Series C: Dynamics, Control, Robotics, Design and Manufacturing* **37**(4), 755–764 (1994).

14. T. Arai, "Analysis and Synthesis of a Parallel Link Manipulator Based on Its Statics," *J. Robotics Society of Japan* **10**(4), 526–533 (1992) (in Japanese).
15. T. Oiwa and M. Hirano, "Six Degree-of-Freedom Fine Motion Mechanism using Parallel Mechanism – Link Layout Design-," *J. the Japan Society for Precision Engineering* **65**(10), 1425–1429 (1999) (in Japanese).
16. C. Gosselin, "Stiffness Mapping for Parallel Manipulator," *IEEE Trans. on Robotics and Automation* **6**(3), 377–382 (1990).
17. T. Huang, X. Zhao and D. J. Whitehouse, "Stiffness Estimation of a Tripod-Based Parallel Kinematic Machine," *IEEE Trans. on Robotics and Automation* **18**(1), 50–58 (2002).
18. T. Komatsu, M. Uenohara, S. Iikura, H. Miura and I. Shimoyama, "Compliance Control for a Two-Link Flexible Manipulator," *Trans. Japan Society of Mechanical Engineering (C)* **56**(530), 2642–2648 (1990) (in Japanese).
19. F. Pierrot, M. Uchiyama, P. Dauchez and A. Fournier, "A New Design of a 6-DOF Parallel Robot," *J. Robotics and Mechatronics* **2**(4), 308–315 (1991).